

## Four-Body Strange-Particle Production in $pp$ Collisions at 6 BeV/c<sup>†</sup>

S. KLEIN,\* W. CHINOWSKY, R. R. KINSEY,† M. MANDELKERN,§ AND J. SCHULTZ§

*Physics Department and Lawrence Radiation Laboratory, University of California, Berkeley, California 94720*

AND

T. H. TAN||

*Stanford Linear Accelerator Center, Stanford, California 94305*

(Received 24 October 1969)

An exposure of the LRL 72-in. liquid-hydrogen bubble chamber to 6-BeV/c protons has yielded some 3000 examples of production of strange particles in four-body final states. Cross sections for the reactions  $pp \rightarrow \Lambda p K^0 \pi^+$ ,  $pp \rightarrow \Lambda p K^+ \pi^0$ , and  $pp \rightarrow \Lambda n K^+ \pi^+$  are  $64 \pm 6 \mu\text{b}$ ,  $39 \pm 6 \mu\text{b}$ , and  $43 \pm 4 \mu\text{b}$ , respectively. The resonances  $K^*(890)$ ,  $N^*(1236)$ , and  $Y^*(1385)$  are produced with cross sections  $\sigma(pK^{*+}) = 9 \pm 3 \mu\text{b}$ ,  $\sigma(\Lambda^0 K^0 N^{*++}) = 23 \pm 3 \mu\text{b}$ ,  $\sigma(\Delta K^+ N^{*+}) = 4 \pm 2 \mu\text{b}$ ,  $\sigma(pK^0 Y^{*+}) = 11 \pm 2 \mu\text{b}$ ,  $\sigma(pK^+ Y^{*0}) = 7 \pm 1 \mu\text{b}$ , and  $\sigma(nK^+ Y^{*+}) = 15 \pm 2 \mu\text{b}$ . Except for the low- $K\pi$ -effective-mass region, the data are found to be in good agreement with a pion-exchange model.

### I. INTRODUCTION

THE inelastic proton-proton interaction<sup>1</sup> has been studied most extensively in reactions yielding nonstrange particles. Those results indicate that resonance production is dominant and that the reactions can often be interpreted as examples of pseudo-two-body production. Single-pion-exchange models have

<sup>†</sup> Work performed under the auspices of the U. S. Atomic Energy Commission.

\* Present address: Universität Heidelberg, Heidelberg, Germany.

† Present address: Brookhaven National Laboratory, Upton, N. Y.

§ Present address: University of California, Irvine, Calif.

|| Present address: University of Colorado, Boulder, Colo.

<sup>1</sup> Results on production of  $N^*$  resonances in  $pp$  collisions, using missing-mass spectrometer techniques, are reported in K. J. Foley, R. S. Jones, S. J. Lindenbaum, W. A. Love, S. Ozaki, E. D. Platner, C. A. Quarles, and E. H. Willen, *Phys. Rev. Letters* **19**, 397 (1967); I. M. Blair, A. E. Taylor, W. S. Chapman, P. I. P. Kalmus, J. Litt, M. C. Miller, D. B. Scott, H. J. Sherman, A. Astbury, and T. G. Walker, *ibid.* **17**, 789 (1966); E. W. Anderson, E. J. Bleser, G. B. Collins, T. Fujii, J. Menes, F. Turkot, R. A. Carrigan, Jr., R. M. Edelstein, N. C. Hien, T. J. McMahon, and I. Nadelhaft, *ibid.* **16**, 855 (1966); C. M. Ankenbrandt, A. R. Clyde, B. Cork, D. Keefe, L. T. Kerth, W. M. Layson, and W. A. Wenzel, *Nuovo Cimento* **35**, 1052 (1965); G. Cocconi, E. Lillethun, J. P. Scanlon, C. A. Stahlbrandt, C. C. Ting, J. Walters, and A. M. Wetherell, *Phys. Letters* **8**, 134 (1964); G. G. Chadwick, G. B. Collins, P. J. Duke, T. Fujii, N. C. Hein, M. A. R. Kemp, and F. Turkot, *Phys. Rev.* **128**, 1823 (1962); G. Cocconi, A. N. Diddens, E. Lillethun, G. Manning, A. E. Taylor, T. G. Walker, and A. M. Wetherell, *Phys. Rev. Letters* **7**, 450 (1961).

Results on pion production in  $pp$  collisions are contained in D. V. Bugg, A. J. Oxley, J. A. Zoll, J. G. Rushbrooke, V. E. Barnes, J. B. Kinson, W. P. Dodd, G. A. Doran, and L. Riddiford, *Phys. Rev.* **133**, B1017 (1964); A. P. Colleraine and U. Nauenberg, *ibid.* **161**, 1387 (1967); S. Coletti, J. Kidd, L. Mandelli, V. Pelosi, S. Ratti, V. Russo, L. Tallone, E. Zampieri, C. Caso, F. Conte, M. Dameri, C. Grosso, and G. Tomasini, *Nuovo Cimento* **49A**, 479 (1967); A. M. Eisner, E. L. Hart, R. I. Louttit, and T. W. Morris, *Phys. Rev.* **138**, B670 (1965); E. L. Hart, R. I. Louttit, D. Luers, T. W. Morris, W. J. Willis, S. S. Yamamoto, *ibid.* **126**, 747 (1962); W. J. Fickinger, E. Pickup, D. K. Robinson, and E. O. Salant, *ibid.* **125**, 2082 (1962); E. Pickup, D. K. Robinson, and E. O. Salant, *ibid.* **125**, 2091 (1962); G. A. Smith, H. Courant, E. C. Fowler, H. Kraybill, J. Sandweiss, and H. Taft, *ibid.* **123**, 2160 (1961); R. R. Kinsey, Ph.D. thesis, UCRL Report No. UCRL-17707, 1968 (unpublished); E. Gellert, G. A. Smith, S. Wojcicki, E. Colton, P. E. Schlein, and H. K. Ticho, *Phys. Rev. Letters* **17**, 884 (1966); E. Colton, P. E. Schlein, E. Gellert, and G. A. Smith, *ibid.* **21**, 1548 (1968); see also Ref. 2.

been generally successful in interpreting these data. Until recently, the strange-particle data have been too sparse for any detailed analysis. The three-body strange-particle final states have been investigated, and the reported results indicate that pion exchange is probably an important mechanism in their production.<sup>2-8</sup> The four-body strange states have been only incompletely or qualitatively studied previously.<sup>2,3,5</sup>

We present results for the reactions

- (a)  $pp \rightarrow \Lambda p K^0 \pi^+$ ,
- (b)  $\quad \rightarrow \Lambda p K^+ \pi^0$ ,
- (c)  $\quad \rightarrow \Lambda n K^+ \pi^+$ ,

produced by 6-BeV/c protons incident on the Alvarez 72-in. liquid-hydrogen bubble chamber. Details of the 550 000-picture exposure at the Bevatron at UCLRL have been presented in another paper<sup>4</sup> reporting results of the experiment and will not be repeated here. We find  $Y^*(1385)$  resonance production in all three final states and  $N^*(1236)$  and  $K^*(890)$  production in reactions (a) and (b). A low-mass enhancement in the  $Y^*K$  system is observed in all reactions and has been interpreted as  $N^*(1950)$  production proceeding via pion exchange. The latter result has been previously reported.<sup>9</sup>

<sup>2</sup> G. Alexander, O. Benary, G. Czapek, B. Haber, N. Kidron, B. Reuter, A. Shapira, E. Simopoulou, and G. Yekutieli, *Phys. Rev.* **154**, 1284 (1967).

<sup>3</sup> G. Alexander, A. Shapira, E. Simopoulou, and G. Yekutieli, *Nuovo Cimento* **53A**, 455 (1968).

<sup>4</sup> W. Chinowsky, R. R. Kinsey, S. L. Klein, M. Mandelkern, J. Schultz, F. Martin, M. L. Perl, and T. H. Tan, *Phys. Rev.* **165**, 1466 (1968).

<sup>5</sup> E. Bierman, A. P. Colleraine, and U. Nauenberg, *Phys. Rev.* **147**, 922 (1966).

<sup>6</sup> W. M. Dunwoodie, H. K. Ticho, G. A. Smith, and A. B. Wicklund, UCLA Report No. UCLA-1031 (unpublished).

<sup>7</sup> M. Firebaugh, G. Ascoli, E. L. Goldwasser, R. D. Sard, and J. Wray, *Phys. Rev.* **172**, 1354 (1968).

<sup>8</sup> T. Yao, *Phys. Rev.* **125**, 1048 (1962).

<sup>9</sup> W. Chinowsky, P. Condon, R. R. Kinsey, S. Klein, M. Mandelkern, P. Schmidt, J. Schultz, F. Martin, M. L. Perl, and T. H. Tan, *Phys. Rev.* **171**, 1421 (1968).

## II. PROCESSING OF EVENTS

All the film was scanned once, and approximately three-fourths of it was rescanned. The topologies used in this analysis were two-pronged events with either one or two visible neutral  $V^0$ 's. Events were measured with either Franckenstein or Vanguard measuring machines and fitted using the two-view reconstruction and fitting program PACKAGE. A small subsample of events was also processed with the three-view TVGR-SQUAW program to check for possible biases in the fitting procedure. The identification of events in the two cases was invariably the same.

Examples of the reaction  $pp \rightarrow \Sigma^0 p K^0 \pi^+$  were not included in the analysis because of the small number of events and rather serious biases. A fit to either (b) or (c) was accepted if the  $V^0$  fitted the three-constraint (3C)  $\Lambda$  hypothesis and if the 1C fit for the production hypothesis had a  $\chi^2$  less than 5.0. For reaction (a), events with two visible  $V^0$  decays were accepted if the corresponding 4C fit to the production hypothesis had a confidence level greater than 0.005. In all cases, the predicted bubble densities for the two charged tracks at the production vertex were required to be compatible with those observed. Events which, after repeated measurement, failed to fit kinematics of one of the four-body reactions were considered to have two or more unobserved neutrals.

Except for a negligible number, all fitting ambiguities are among production hypotheses with the same observed neutral particle. Except for ambiguities between the 4C fit  $\Delta p K^0 \pi^+$  and the 2C fit  $\Sigma^0 p K^0 \pi^+$ , which are discussed below, events ambiguous among fits of different constraint class were assigned to the hypothesis of higher constraint. In Table I we give the observed number of events for each of the various categories.

TABLE I. Event totals and cross sections for  $pp$  four-body reactions containing a  $\Lambda$ .

Category	Observed No. of events	Corrected No. of events <sup>a</sup>	Cross section ( $\mu\text{b}$ )
$\Delta p K^0 \pi^+$	959	990	$64 \pm 6$
$\Sigma^0 p K^0 \pi^+$	160	164	$11 \pm 2$
$\Delta p K^+ \pi^0$	492	531	$39 \pm 6$
$\Delta n K^+ \pi^+$	554	614	$43 \pm 4$
$\Delta p K^0 \pi^+ - \Sigma^0 p K^0 \pi^+$	59	42	
$\Delta p K^0 \pi^+ - \Delta p K^+ \pi^0$	71	71	
$\Delta p K^0 \pi^+ - \Delta n K^+ \pi^+$	41	36	
$\Delta p K^+ \pi^0 - \Delta K^+ p \pi^0$	20	19	
$\Delta n K^+ \pi^+ - \Delta n \pi^+ K^+$	50	55	
$\Lambda +$ (two-prong)	1148	1275	
+two or more missing neutrals			

<sup>a</sup> These are the corrected numbers of events after minimum-length and projected-opening-angle cuts and corresponding weightings have been applied to the data.

## III. CROSS SECTIONS

Corrections to the observed numbers of events were made to accommodate observational biases. The observed proper lifetime distributions for both  $\Lambda$ 's and  $K^0$ 's are depleted for times  $t < 0.2\tau$ , where  $\tau$  is the mean lifetime, because of low efficiency for detection of  $V^0$  decays near the production vertex. A minimum-decay-length cutoff of 1.2 cm and a corresponding weighting were applied to the sample to correct for this effect. Evidence for bias against  $\Lambda$ 's with small projected opening angle was found in the angular distribution of the  $\Lambda$  decay. We define  $\phi$  to be the angle between the plane of the decay and a plane containing the  $\Lambda$  direction and a vector perpendicular to the plane of the chamber. Deviations from isotropy were observed in

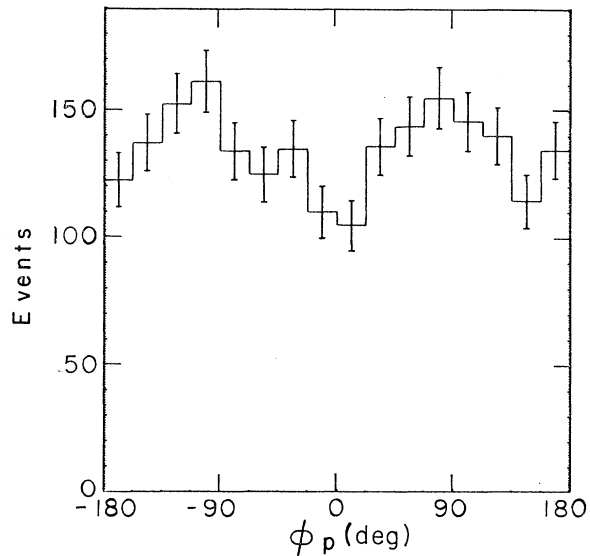


FIG. 1. Azimuth angle distribution of the decay proton for all  $\Lambda$ 's with path length greater than 1.2 cm.

the distribution in  $\phi$  (Fig. 1), indicating a bias against small projected opening angles. Only events with projected opening angle greater than  $3^\circ$  were retained and weighted appropriately. The average weights for the length and projected opening angle corrections are 1.11 and 1.23, respectively. Table I gives the corrected number of events. Study of the  $K^0$  decay distributions indicated an additional bias against detection of slow  $K^0$ 's. Disagreement with the expected branching ratios of 1:4:2 for  $(\Lambda)pK^0\pi^+ : \Delta p(K^0)\pi^+ : \Delta pK^0\pi^+$ , where parentheses denote an unobserved neutral, reflects this bias. Reexamination of events which fit  $pp \rightarrow \Lambda p(K^0)\pi^+$  with missing  $K^0$  momentum less than 500 MeV/c revealed missed decays in the chamber volume. After correction, the ratios of cross sections are satisfactory. Events were not weighted to correct for this bias, since only 30 events were completely missing from the sample of

1000 events and no biases in effective-mass distributions were indicated.

The center-of-mass reflection symmetry of proton-proton collisions was exploited to determine evidence for biases in the data. First, we present evidence in Fig. 2(a) that the criteria for the assignment of events to the category of two missing neutrals gives a sample consistent with center-of-mass symmetry. This shows the distribution in the cosine of the  $\Lambda$  production angle in the over-all center-of-mass system using weighted events. The reference direction is defined by the beam proton. About half of the entire sample of events are in this histogram. The normalized curve is a rough fit to the data and is included only to indicate agreement with symmetry. Figure 2(b) shows the production angular distribution for  $\Lambda$ 's in all the identified final states. Events of the channel  $\Lambda n K^+ \pi^+$  show the greatest departure from reflection symmetry, as seen in the  $\Lambda$  production angular distribution of Fig. 2(c). A scatter plot of  $\cos\theta_\Lambda$  versus  $\cos\theta_n$ , where  $\theta_\Lambda$  and  $\theta_n$  are the center-of-mass production angles with respect to the beam proton, shows 730 events with  $\Lambda$  and  $n$  in opposite hemispheres. Of these, 360 have  $\cos\theta_\Lambda > 0$ , and 370 have  $\cos\theta_\Lambda < 0$ , consistent with reflection symmetry. Of the 178 events with  $\Lambda$  and  $n$  in the same hemispheres, only 60 have the two baryons together in the forward hemisphere. This is essentially the complete observed asymmetry. A source of contamination is the five-body state  $\Lambda p \pi^+ (K^0 \pi^0)$ . About 150 examples of this reaction have been obtained with both  $K^0$  and  $\Lambda$  decays observed. The fraction of these events which fitted the  $\Lambda(n)K^+ \pi^+$  hypothesis, after eliminating the  $K^0$  decay measurement, and which were consistent with the bubble densities, indicates that the asymmetry can be solely accounted for by contamination from the channel  $\Lambda p \pi^+ (K^0 \pi^0)$ . Except for three of 27 events, this falsely identified sample populated only that quadrant having the event excess, i.e., that defined by  $\cos\theta_n < 0$  and  $\cos\theta_\Lambda < 0$ . These events showed no other significant deviations from the effective-mass and angular distributions of the true events. Therefore, for the  $\Lambda(n)K^+ \pi^+$  final state, only the cross section was corrected. In addition to those five-body events which fitted the  $\Lambda n K^+ \pi^+$  hypothesis after removal of the  $K^0$ , a smaller number fitted the  $\Lambda p K^+ \pi^0$  hypothesis. This sample was statistically insufficient for studying differential biases. Besides this source and the  $pp \rightarrow \Sigma^0 p K^+$  events ambiguous with the hypothesis  $\Lambda p K^+ \pi^0$ , we expect the  $\Lambda p K^+ \pi^0$  and the  $\Lambda n K^+ \pi^+$  events to be contaminated by four-body final states with  $\Sigma^0$ 's. Unfortunately, cross sections for  $pp \rightarrow \Sigma^0 p K^+ \pi^-$ ,  $\Sigma^0 n K^+ \pi^+$  are unknown, so the magnitude of this contamination cannot be determined. With the assumption that the relative production rate of  $\Sigma^0$  and  $\Lambda$  for each of these two four-body  $K^+$  states is the same as in the final states  $\Sigma^0 p K^0 \pi^+$  and  $\Lambda p K^0 \pi^+$  and that their production mechanisms are similar, the  $\Sigma^0$  contamination in these  $K^+$  states is expected to be

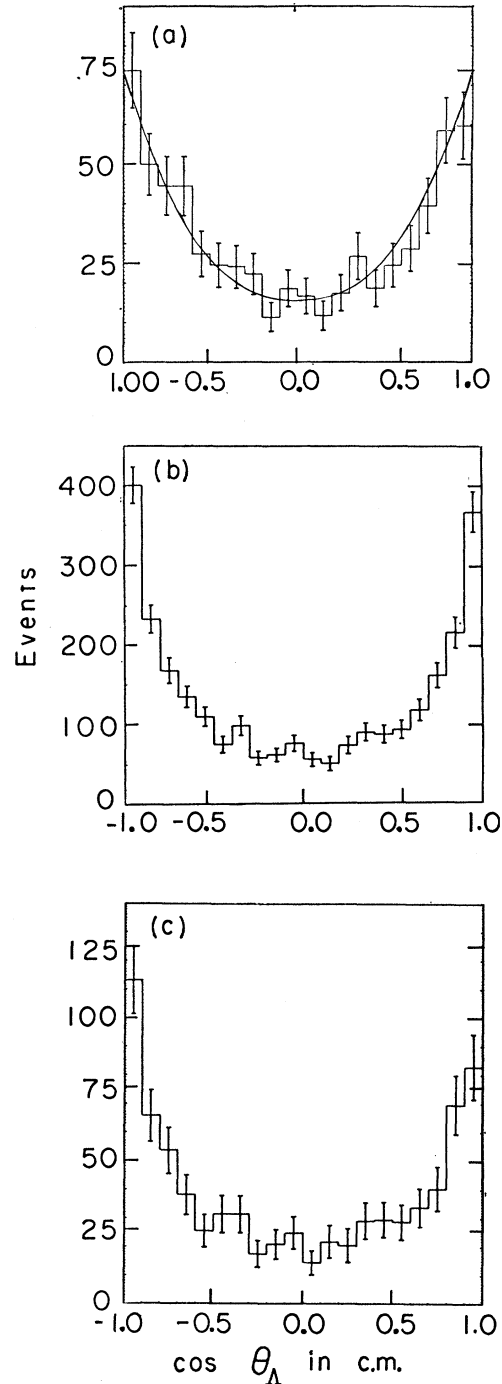


FIG. 2. Production angular distribution in the  $pp$  center-of-mass system for (a) events with two or more missing neutral particles, (b) all four-body events with a visible  $\Lambda$ , and (c) events identified as  $pp \rightarrow \Lambda n K^+ \pi^+$ .

less than 8%. This number is based on the assumption that all of the ambiguities between  $\Lambda p K^0 \pi^+$  and  $\Sigma^0 p K^0 \pi^+$  belong to the latter category and, hence, is likely to be an overestimate. In fact, judging from the center-of-

mass angular distribution for  $\Lambda p K^0 \pi^+$  production, it is probable that most of those events are truly  $\Lambda$  events. We have shown in a previous article<sup>4</sup> that this is the case for  $\Lambda p K^+ \Sigma^0 p K^+$  ambiguous events. Events ambiguous between two kinematic hypotheses are included in both categories with a weighting factor of  $\frac{1}{2}$ . No significant changes in mass and angular distributions are observed when this factor is varied from 0 to 1. The biases we have discussed contribute relatively small numbers of events compared to the totals.

Beam tracks were counted in 1000 frames evenly spaced throughout the film yielding  $5\,090\,000 \pm 150\,000$  for the total number of noninteracting protons. The uncertainty given is not the statistical error but rather the average deviation of several measurements. Using a fiducial length of 125 cm, total  $pp$  interaction cross section 40.6 mb,<sup>10</sup> and target proton density of  $(0.361 \pm 0.007) \times 10^{23}/\text{cm}^3$ , we obtain  $\sigma_i = N_i(0.0401 \pm 0.0014) \mu\text{b}$  as the partial cross section for channel  $i$ .  $N_i$  is the sum of the weights for the events in the channel and the uncertainty in  $N_i$  is

$$\left(\sum_j w_j^2\right)^{1/2},$$

where  $w_j$  is the weight for the  $j$ th event. In making the path length determination, we have used 1.6 mb<sup>11</sup> as the cross section for unobserved low-momentum-transfer elastic scatters. Comparing two independent scans, an efficiency of  $0.96 \pm 0.02$  was found. The production cross sections obtained for the various final states are given in Table I.

#### IV. RESONANCE PRODUCTION

Since the three final states  $\Lambda p K^0 \pi^+$ ,  $\Lambda p K^+ \pi^0$ , and  $\Lambda n K^+ \pi^+$  each contain the same hadrons differing only in their charges, we expect the dynamical mechanisms of their production to be related. With few exceptions, we indeed find the same general behavior in the data for each state. Therefore, we discuss the three final states simultaneously.

In Figs. 3–5 we display the various  $N\pi$ ,  $\Lambda\pi$ , and  $K\pi$  effective-mass spectra. All the established pionic resonances,  $Y^*(1385)$ ,  $K^*(890)$ , and  $N^*(1236)$ , are present. We find evidence in all channels for peripheral production of  $N_{3/2}^*(1950)$  with subsequent decay into  $Y^*K$ . Analysis of this reaction has been presented elsewhere.<sup>9</sup>

In order to estimate the relative production rates of the pionic resonances, we have fitted the data for each final state to a sum of pure phase-space plus resonance production. Although certain features of the data are certainly in disagreement with the simplifying assumptions of isotropic production and decay of resonances, we nevertheless are able to estimate reliably the relative cross sections for  $N^*$ ,  $K^*$ , and  $Y^*$  production.

<sup>10</sup> R. F. George, K. F. Riley, R. J. Tapper, D. V. Bugg, D. C. Salter, and G. H. Stafford, Phys. Rev. Letters 15, 214 (1965).

<sup>11</sup> A. R. Clyde, Ph.D. thesis, UCRL Report No. UCRL-16275 (unpublished).

In four-body production where no correlation of the final state with the initial state is included, five independent variables are necessary to specify the final

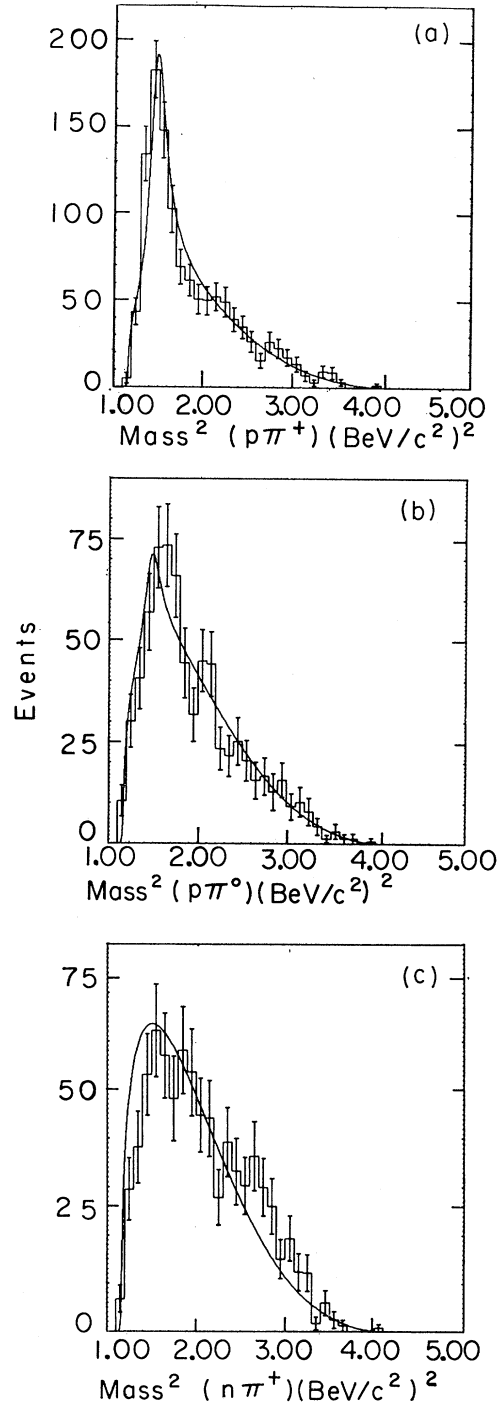


FIG. 3. Square of the effective mass of the  $N\pi$  combination for the final states (a)  $\Lambda p K^0 \pi^+$  (1170 events), (b)  $\Lambda p K^+ \pi^0$  (708 events), and (c)  $\Lambda n K^+ \pi^+$  (791 events). The curves are the theoretical distributions calculated with the phase-space plus resonance model described in the text.

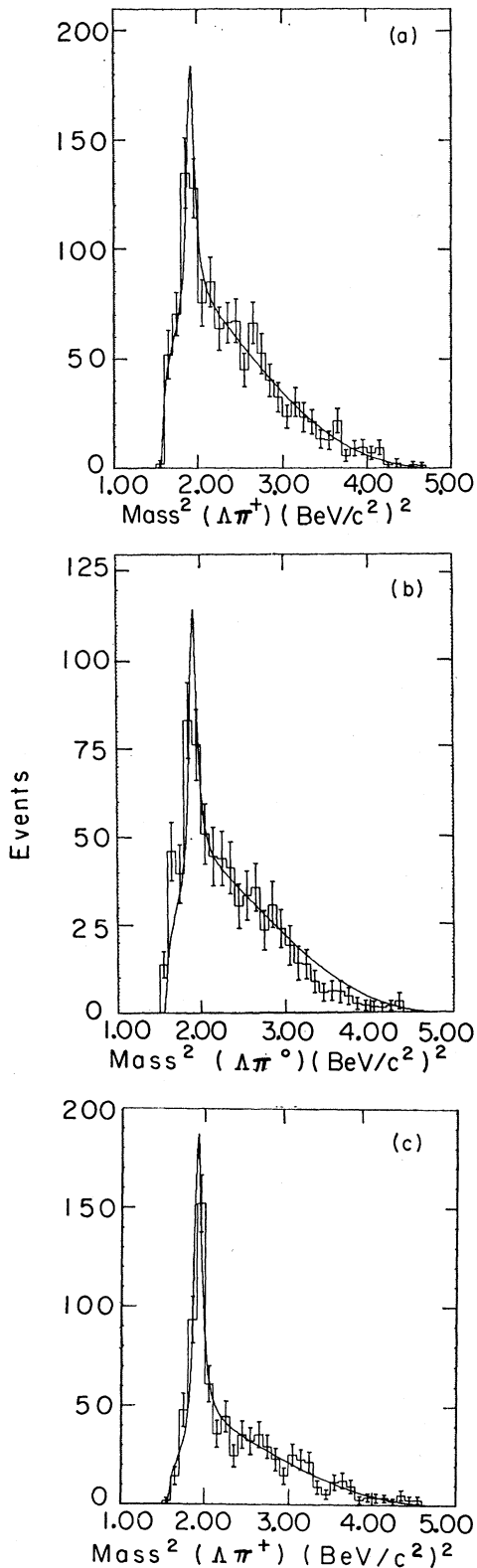


FIG. 4. Square of the effective mass of the  $\Delta\pi$  combination for the final states (a)  $\Delta p K^0 \pi^+$ , (b)  $\Delta p K^+ \pi^0$ , and (c)  $\Delta n K^+ \pi^+$ . The curves show theoretical distributions obtained with the phase-space plus resonance model.

state. For each final state the experimental density was fitted to a function of the five kinematic variables, consisting of an incoherent sum of terms representing reso-

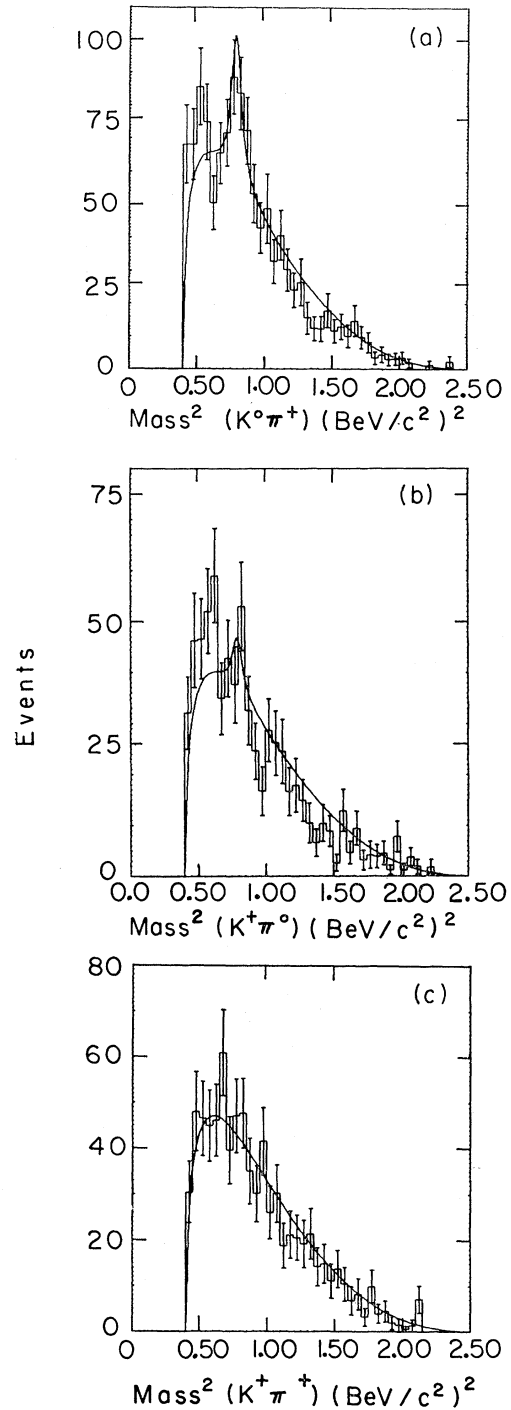


FIG. 5. Square of the effective mass of the  $K\pi$  combination for the final states (a)  $\Delta p K^0 \pi^+$ , (b)  $\Delta p K^+ \pi^0$ , and (c)  $\Delta n K^+ \pi^+$ . The curves show theoretical distributions obtained with the phase-space plus resonance model.

nant processes and phase space,

$$f(x) = \sum_{j=1}^N \alpha_j |M_j(x)|^2 \rho(x). \quad (1)$$

The  $\alpha_j$  are the relative intensities of the different processes,  $x$  denotes the set of five independent variables, the  $|M_j|^2$  are proportional to the corresponding Lorentz-invariant matrix elements squared, and  $\rho(x)$  is the phase-space density. The normalization conditions are

$$\int |M_j(x)|^2 \rho(x) dx_1 \cdots dx_5 = 1 \quad \text{for each } j \quad (2)$$

and

$$\sum_{j=1}^N \alpha_j = 1. \quad (3)$$

The  $\alpha_j$  were determined by a maximum-likelihood method.

For the  $N^*(1236)$ ,  $K^*(890)$ , and  $Y^*(1385)$  resonance terms, we use

$$|M_j|^2 = \text{const} \frac{m^2}{p} \frac{\Gamma(m)}{(m^2 - m_0^2)^2 + m_0^2 \Gamma^2(m)}, \quad (4)$$

where  $m$  is the invariant mass of the resonant pair of particles and  $p$  is the momentum of either one in the rest frame of  $m$ . The total width is used both in the denominator and numerator, since all the resonances are nearly elastic. The constants are determined by the normalization conditions above. For  $N^*(1236)$  and  $Y^*(1385)$ , we use

$$\frac{\Gamma(m)}{\Gamma(m_0)} = \left(\frac{p}{p_0}\right)^3 \frac{m_0}{m} \frac{E_B + m_B}{E_B^0 + m_B}, \quad (5)$$

where  $E_B$  is the energy of the baryon in the resonance rest system,  $m_B$  is the mass of the baryon, and  $p_0$  and  $E_B^0$  are the values of  $p$  and  $E_B$  at the nominal resonance mass  $m_0$ . For  $K^*(890)$ , we use

$$\frac{\Gamma(m)}{\Gamma(m_0)} = \left(\frac{p}{p_0}\right)^3 \left(\frac{m_0}{m}\right)^2. \quad (6)$$

Table II gives the results of fits for the relative intensities and corresponding cross sections. The errors quoted are estimates of the precision with which we determine the various relative intensities. The resonance cross sections are seen to be in reasonable agreement with charge-independence requirements, which predict ratios of 9:2:1 for

$$\Lambda K^0(N^{*++} \rightarrow p\pi^+) : \Delta K^+(N^{*+} \rightarrow p\pi^0) : \Delta K^+(N^{*+} \rightarrow n\pi^+)$$

and 2:1 for

$$(K^{*+} \rightarrow K^0\pi^+) : (K^{*+} \rightarrow K^+\pi^0).$$

TABLE II. Resonance cross sections for  $p\bar{p} \rightarrow \Lambda N K \pi$  at 6 BeV/c.

	$Y^*(1385)$	$N^*(1236)$	$K^*(890)$	Background
$\Lambda p K^0 \pi^+$				
Relative fraction	$0.18 \pm 0.02$	$0.36 \pm 0.04$	$0.10 \pm 0.03$	$0.36 \pm 0.04$
Cross section ( $\mu\text{b}$ )	$11 \pm 2$	$23 \pm 3$	$6 \pm 2$	$23 \pm 3$
$\Delta p K^+ \pi^0$				
Relative fraction	$0.19 \pm 0.03$	$0.10 \pm 0.04$	$0.04 \pm 0.02$	$0.67 \pm 0.04$
Cross section ( $\mu\text{b}$ )	$7 \pm 1$	$4 \pm 2$	$2 \pm 1$	$26 \pm 4$
$\Lambda n K^+ \pi^+$				
Relative fraction	$0.34 \pm 0.02$	$0.0 \pm 0.03$	...	$0.66 \pm 0.03$
Cross section ( $\mu\text{b}$ )	$15 \pm 2$	$0 \pm 1$	...	$29 \pm 3$

The curves superimposed on the experimental histograms of Figs. 3–5 show the mass distributions obtained with this model. Except for the  $K^0\pi^+$  and  $K^+\pi^0$  mass distributions, the agreement is excellent. The enhancements seen in the low- $(K\pi)^+$ -mass region correspond to a mass of 725 MeV/ $c^2$  and a width of 70 MeV/ $c^2$ . There have been similar observations in different experiments, but interpretation of them as evidence for a resonance has been generally unconvincing because of inconsistencies in production rates and observed widths.<sup>12</sup> It is possible that the effects are dynamically correlated with  $N^*(1236)$  or  $Y^*(1385)$  production. Lack of an enhancement in the  $K^+\pi^+$  mass distribution for the  $\Delta K^+\pi^+$  state, where  $Y^*(1385)$  production is strongest, tends to rule out  $Y^*(1385)$  as a source. It may be important that the  $K\pi$  enhancement is largest in the state where  $N^*(1236)$  production is dominant, and absent in the state where no  $N^*(1236)$  is observed. Of course, a  $K\pi$  interaction in  $I = \frac{1}{2}$  only would also account for this observation. In the corresponding predictions of pion-exchange model

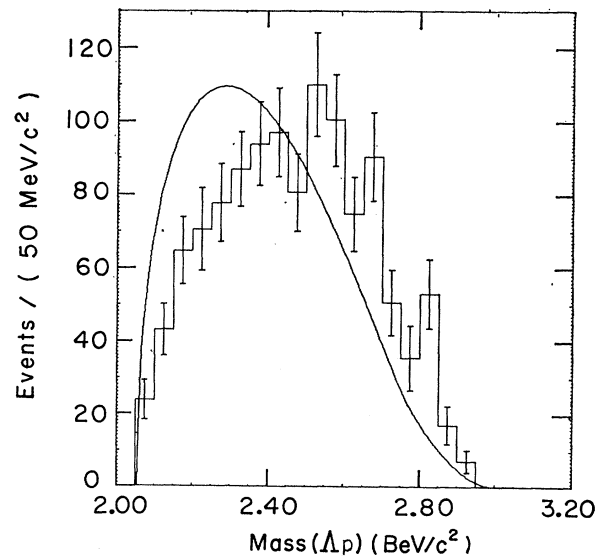


FIG. 6. Effective mass of the  $\Lambda p$  combination for the final state  $\Lambda p K^0 \pi^+$ . The distribution obtained with the phase-space plus resonance model is shown in the smooth curve.

<sup>12</sup> N. Barash-Schmidt, A. Barbaro-Galtieri, L. R. Price, A. H. Rosenfeld, P. Söding, C. G. Wohl, M. Roos, and G. Conforto, *Rev. Mod. Phys.* **41**, 109 (1969).

discussed below, the  $K^0\pi^+$  mass distribution [displayed in Fig. 12(f)] fails to indicate any peaking in the low- $K\pi$ -mass region.

The  $K\pi$ ,  $N\pi$ , and  $\Lambda\pi$  effective-mass distributions are in rather good agreement with the above model. Since we assume isotropic production and decay of resonances, we expect angular distributions and some effective-mass distributions not to agree with the model. The  $\Lambda N$  mass distributions are in gross disagreement; for example Fig. 6 gives the  $\Lambda p$  mass distribution for the  $\Lambda p K^0\pi^+$  final state.

### V. ONE-PION EXCHANGE

Those features of the data which are sensitive to the production and decay angular distributions of the resonances can be included in the framework of a single-particle-exchange model. Although several particle-exchange processes can contribute to the amplitude for each reaction, we make the assumption that only pion exchange is present and do not consider other processes such as kaon exchange. We have shown in an earlier paper that pion exchange alone is a good description for three-body strange-particle final states. The exchange model is found to give a satisfactory description of the present data as well.

Figure 7 shows the possible single-pion-exchange diagrams. The diagram of Fig. 7(a) requires fewest assumptions for the calculation, since the vertices involve only two-body scattering processes. The  $N\pi$  cross sections are known very well, and the  $\Lambda K$  cross section has been fairly well studied. The amplitude of diagram 7(b) can be separated into contributions from Figs. 7(c)–7(e), assuming that the only resonances produced are  $K^*(890)$  and  $Y^*(1385)$ . The cross section for a final state is then calculated as an incoherent sum of squares of the corresponding amplitudes for the four diagrams (a), (c)–(e). Contribution to the amplitude from the diagram obtained by interchange of the two initial-state protons is included. This gives just a factor of 2 in the cross section with the neglect of interference terms, justified by the strongly peripheral character of the reactions.

For the calculation of the diagram 7(a), we follow Salzman and Salzman<sup>13</sup> and assume that both virtual-pion interactions can be represented by the real-pion cross sections at the same total energy. The differential cross section is then

$$\frac{d^7\sigma}{dm_{N\pi}^2 dm_{\Lambda K}^2 dt d\cos\theta_{N\pi} d\phi_{N\pi} d\cos\theta_{\Lambda K} d\phi_{\Lambda K}} = \frac{1}{32\pi^3} \frac{1}{(\vec{p}\vec{E})^2} \frac{1}{(t+\mu^2)^2} \frac{d\sigma_{N\pi}}{d\Omega_{N\pi}} k_{N\pi} m_{N\pi} \frac{d\sigma_{\Lambda K}}{d\Omega_{\Lambda K}} k_{\Lambda K} m_{\Lambda K}. \quad (7)$$

Here  $m_{N\pi}$  and  $m_{\Lambda K}$  are the effective masses of the pairs of particles,  $t$  is the square of the four-momentum transfer between the initial proton and the  $N\pi$  system,

<sup>13</sup> F. Salzman and G. Salzman, Phys. Rev. 121, 1541 (1961).

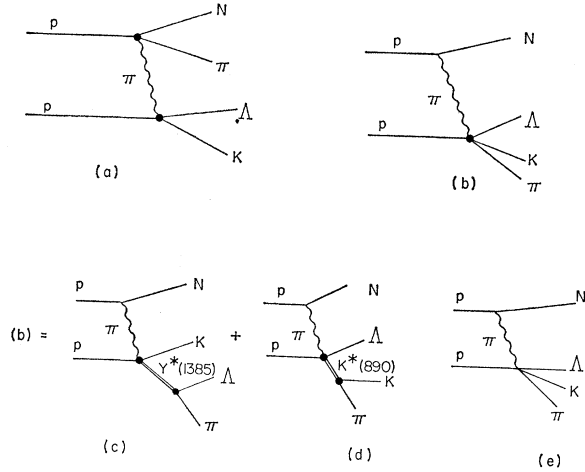


FIG. 7. One-pion-exchange diagrams used in the calculations.

$\theta_{N\pi}$  is the angle between the initial proton and the final-state nucleon in the  $N\pi$  rest system, and  $\phi_{N\pi}$  is the corresponding azimuthal angle of the nucleon about the initial proton direction;  $\theta_{\Lambda K}$  and  $\phi_{\Lambda K}$  are defined analogously to  $\theta_{N\pi}$  and  $\phi_{N\pi}$ ;  $\vec{p}$  and  $\vec{E}$  are the momentum and energy of either initial-state proton in the over-all center-of-mass system;  $d\sigma_{N\pi}/d\Omega_{N\pi}$  and  $d\sigma_{\Lambda K}/d\Omega_{\Lambda K}$  are the experimental differential cross sections for  $\pi p \rightarrow N\pi$  and  $\pi p \rightarrow \Lambda K$ , respectively;  $k_{N\pi}$  and  $k_{\Lambda K}$  are the momenta of real pions in the center-of-mass system for the reactions  $\pi p \rightarrow N\pi$  and  $\pi p \rightarrow \Lambda K$  at total energies  $m_{N\pi}$  and  $m_{\Lambda K}$ , respectively.

The experimental  $\pi p \rightarrow \pi N$  cross sections were calculated from a recent phase-shift analysis.<sup>14</sup> In the energy range needed for our four-body states, these cross sections are dominated by  $N^*(1236)$  production. The various  $\pi p \rightarrow \Lambda K$  differential cross sections we use are taken from reports listed in Ref. 15.

For the process describing  $Y^*(1385)$  production, we use

$$\frac{d^7\sigma}{dm_{\Lambda\pi}^2 dm_{\Lambda K}^2 dt d\cos\theta_{\Lambda\pi} d\phi_{\Lambda\pi} d\cos\theta_{\Lambda K} d\phi_{\Lambda K}} = \frac{G^2}{4\pi} \frac{1}{16\pi} \frac{e^{-\alpha(t+m_\pi^2)t}}{(t+m_\pi^2)^2} \frac{1}{(\vec{p}\vec{E})^2} \frac{d\sigma_{Y^*}}{d\Omega} (w, \theta_{\Lambda\pi}) \times \frac{\hat{p}_\Lambda}{m_{\Lambda\pi}} \frac{\hat{p}_{\Lambda\pi}}{(m_{\Lambda\pi}^2 - m_0^2)^2 + m_0^2 \Gamma^2} y(w), \quad (8)$$

<sup>14</sup> A. Donnachie, R. G. Kirsopp, and C. Lovelace, Phys. Letters 26B, 161 (1968).

<sup>15</sup> L. Bertanza, P. L. Connolly, B. B. Culwick, F. R. Eisler, T. Morris, R. Palmer, A. Prodell, and N. P. Samios, Phys. Rev. Letters 8, 332 (1962); J. Keren, Phys. Rev. 133, B457 (1964); J. A. Anderson, Ph.D. thesis, UCRL Report No. UCRL-10838 (unpublished); F. Eisler, R. Plano, A. Prodell, N. Samios, M. Schwartz, J. Steinberger, P. Bassi, V. Borelli, G. Puppi, G. Tanaka, P. Woloschek, V. Zobolli, M. Conversi, P. Franzini, I. Mannelli, R. Santangelo, and V. Silvestrini, Phys. Rev. 108, 1353 (1957); Ö. I. Dahl, L. M. Hardy, R. I. Hess, J. Kirz, D. H. Miller, and J. A. Schwartz, *ibid.* 163, 1430 (1967).

where

$$\frac{1}{y(w)} = \int_{(m_\Lambda+m_\pi)^2}^{(w-m_K)^2} \frac{4\pi p_{\Lambda\pi} p_\Lambda}{m_{\Lambda\pi} [(m_{\Lambda\pi}^2 - m_0^2)^2 + m_0^2 \Gamma^2]} dm_{\Lambda\pi}^2. \quad (9)$$

$$G^2/4\pi = 15 \quad \text{for } \pi^0 \text{ exchange}$$

$$= 30 \quad \text{for } \pi^+ \text{ exchange;}$$

$w$  is the effective mass of the  $\Delta K\pi$  system;  $k$  is the c.m. momentum of a real pion in the initial state for  $\pi p \rightarrow \Delta K\pi$  at total energy  $w$ ;  $t$  is the square of the four-momentum transfer between the initial-state proton and the final-state nucleon;  $\theta_{\Delta\pi}$  and  $\phi_{\Delta\pi}$  are the angles describing the  $\Delta\pi$  system defined in the  $\Delta K\pi$  rest system;  $\theta_\Lambda$  and  $\phi_\Lambda$  are the angles describing the  $\Lambda$  in the  $\Delta\pi$  rest system;  $d\sigma_{Y^*}(w, \theta_{\Delta\pi})/d\Omega$  is the differential cross section for  $Y^*(1385)$  production at total energy  $w$ ;  $p_{\Lambda\pi}$  is the momentum of the  $\Delta\pi$  system in the  $\Delta K\pi$  rest system;  $p_\Lambda$  is the momentum of the  $\Lambda$  in the  $\Delta\pi$  rest system;  $m_0$  and  $\Gamma_0$  equal 1.385 BeV/c<sup>2</sup> and 0.040 BeV/c<sup>2</sup>, respectively.

The factor  $e^{-\alpha(t+m_\pi^2)}$  was included to obtain agreement with the four-momentum transfer distribution in the  $nY^*+K^+$  final state. We find  $\alpha = 1.0$  (BeV/c)<sup>-2</sup> adequate for all three final states.

The momentum dependence for the  $Y^*$  decay could also include a  $p$ -wave decay factor, but since the  $Y^*$  is narrow the results are not sensitive to this factor.

Similar expressions are used to describe  $K^*(890)$  production, with resonance parameters  $m_0 = 890$  MeV/c<sup>2</sup> and  $\Gamma_0 = 50$  MeV/c<sup>2</sup>. The factor  $e^{-\alpha(t+m_\pi^2)}$  is omitted as unnecessary for a good fit to the data.

To describe the nonresonant background, we assume  $\pi p \rightarrow \Delta K\pi$  to be described by pure phase space. This assumption is clearly not valid at high values of  $\Delta K\pi$  mass and neglects the low-mass  $\Delta K$  interaction which is

probably present. The background cross section we use is then

$$\frac{d^7\sigma}{dm_{\Lambda\pi}^2 dw^2 dt d\cos\theta_{\Delta\pi} d\phi_{\Delta\pi} d\cos\theta_\Lambda d\phi_\Lambda} = \frac{G^2}{4\pi} \frac{1}{16\pi} \frac{t}{(t+m_\pi^2)^2} \frac{1}{(\vec{p}\vec{E})^2} k w \sigma(w) p_{\Lambda\pi} \frac{p_\Lambda}{m_{\Lambda\pi}} A(w), \quad (10)$$

where

$$\frac{1}{A(w)} = 16\pi^2 \int_{(m_\Lambda+m_\pi)^2}^{(w-m_K)^2} \frac{p_{\Lambda\pi} p_\Lambda}{m_{\Lambda\pi}} dm_{\Lambda\pi}^2 \quad (11)$$

and  $\sigma(w)$  is the  $\pi p \rightarrow \Delta K\pi$  cross section at total energy  $w$ . The other definitions are the same as before.

The energy dependence of the total cross section for  $\pi^0 p \rightarrow Y^*+K^0$ ,  $\pi^0 p \rightarrow Y^*+K^+$ , and  $\pi^0 p \rightarrow \Delta K^*+$ , as well as their angular distributions, are needed for the calculation of production cross sections for the states  $\Lambda p K^0 \pi^+$  and  $\Lambda p K^+ \pi^0$ . In addition,  $\pi^+ p \rightarrow Y^*+K^+$  data are required to calculate the  $\Delta n K^+ \pi^+$  rate. The  $\pi^0$  cross sections were obtained from the following isotopic-spin relations:

$$\sigma(\pi^0 p \rightarrow \Delta K^0 \pi^+) = \sigma(\pi^- p \rightarrow \Delta K^0 \pi^0), \quad (12)$$

and

$$\sigma(\pi^0 p \rightarrow \Delta K^+ \pi^0) = \frac{1}{2} [\sigma(\pi^+ p \rightarrow \Delta K^+ \pi^+) + \sigma(\pi^- p \rightarrow \Delta K^+ \pi^-) - \sigma(\pi^- p \rightarrow \Delta K^0 \pi^0)]. \quad (13)$$

The available data are shown in Figs. 8–11. The smooth curves drawn through the measured values of total cross sections are qualitative representations of the variation with energy. They provide interpolated values of cross sections used in the pion-exchange calculation. Using the experimental data of Fig. 11 for  $\pi^- p \rightarrow \Delta K^* 0$

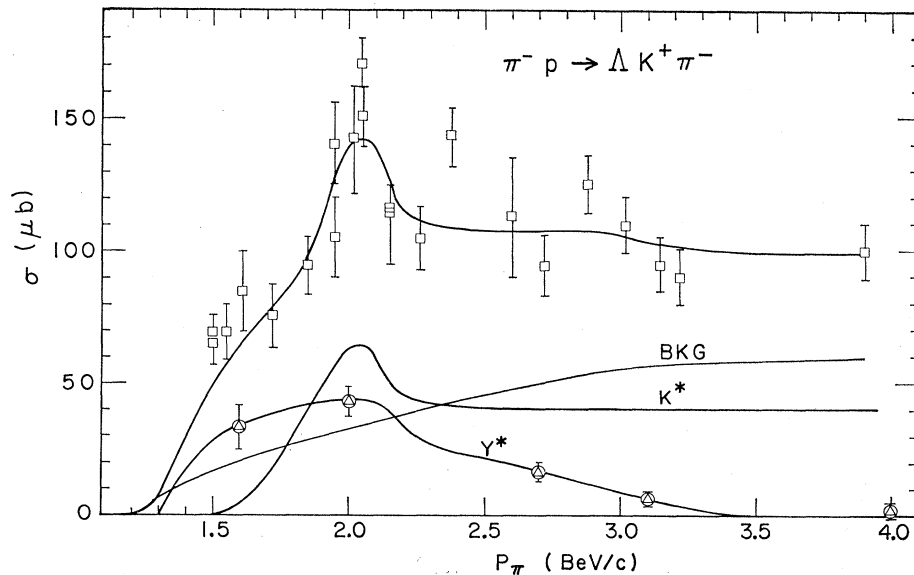


FIG. 8. Cross sections for  $\pi^- p \rightarrow \Delta K^+ \pi^-$  as a function of incident pion lab momentum. Experimental values of total cross sections and  $Y^*$  production are shown. The smooth curves are described in the text.



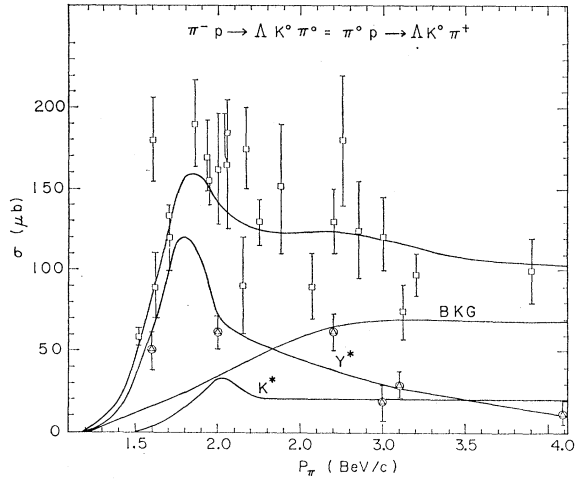


FIG. 9. Cross sections for  $\pi^- p \rightarrow \Lambda K^0 \pi^0 = \pi^0 p \rightarrow \Lambda K^0 \pi^+$  as a function of incident pion lab momentum. Experimental values of total cross sections and  $Y^*$  production are shown. The smooth curves are described in the text.

and charge-independence requirements, the  $K^*$  production cross sections of Figs. 8 and 9 were determined. The curves of the  $Y^*$  production cross section are somewhat crude fits to the sparse available experimental data, and the background curves were obtained by subtraction. No  $\pi^- p \rightarrow Y^* K^0$  production angular distributions are available in the literature. Therefore, we have used angular distributions derived from the present data for  $Y^*$  production. For  $K^*(890)$  production, experimental differential production cross sections are used.

We have fitted the data for each final state to the predictions of the single-pion-exchange model. The relative intensities obtained for the different processes are in excellent agreement with those found in the fit de-

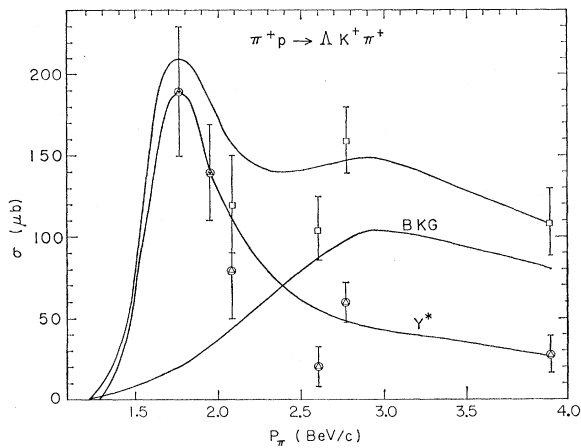


FIG. 10. Cross sections for  $\pi^+ p \rightarrow \Lambda K^+ \pi^+$  versus incident pion lab momentum. Boxes indicate measured total cross sections; inscribed triangles are measured  $Y^*$  production cross sections. At the two lowest momenta, the data are reported to be completely  $Y^* K^+$  production. The curves are described in the text.

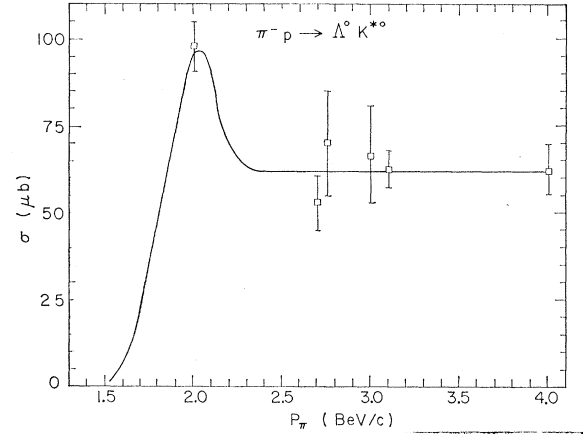


FIG. 11. Total cross sections for  $\pi^- p \rightarrow \Lambda^0 K^{*0}$  versus incident pion lab momentum. The interpolated curve is discussed in the text.

scribed in Sec. IV. The calculated cross sections given in Table III are not in agreement with our measured cross sections. Since one can introduce form factors which do not significantly alter the shapes of distributions, but result in rather different total cross sections, we do not take this discrepancy as evidence of failure of the model.

We compare our experimental distributions with the pion-exchange model. All calculations of experimental quantities, such as scattering angles, which require specification of an initial-state proton were made by associating with any final system that proton with the smallest momentum transfer to the system. This same selection was included in the Monte Carlo calculations. We find less than 15% of the Monte Carlo events required interchange of initial-state protons for the calculation of distributions. In Figs. 12(a)-12(j), we display the six two-body and the four three-body effective-mass distributions for  $\Lambda p K^0 \pi^+$ . We find similar agreement for the other channels not shown. In all the histograms we include the pion-exchange prediction with each contribution separately indicated.

TABLE III. One-pion-exchange predicted cross sections for  $p\bar{p} \rightarrow \Lambda N K \pi$  at 6 BeV/c.

	$Y^*(1385)$ ( $\mu\text{b}$ )	$N^*(1236)$ ( $\mu\text{b}$ )	$K^*(890)$ ( $\mu\text{b}$ )	Background ( $\mu\text{b}$ )
$\Lambda p K^0 \pi^+$	15 (with form factor) 41 (no form factor)	21	28	34
$\Lambda p K^+ \pi^0$	8 (with form factor) 22 (no form factor)	6	14	20
$\Lambda n K^+ \pi^+$	48 (with form factor) 130 (no form factor)	3		46

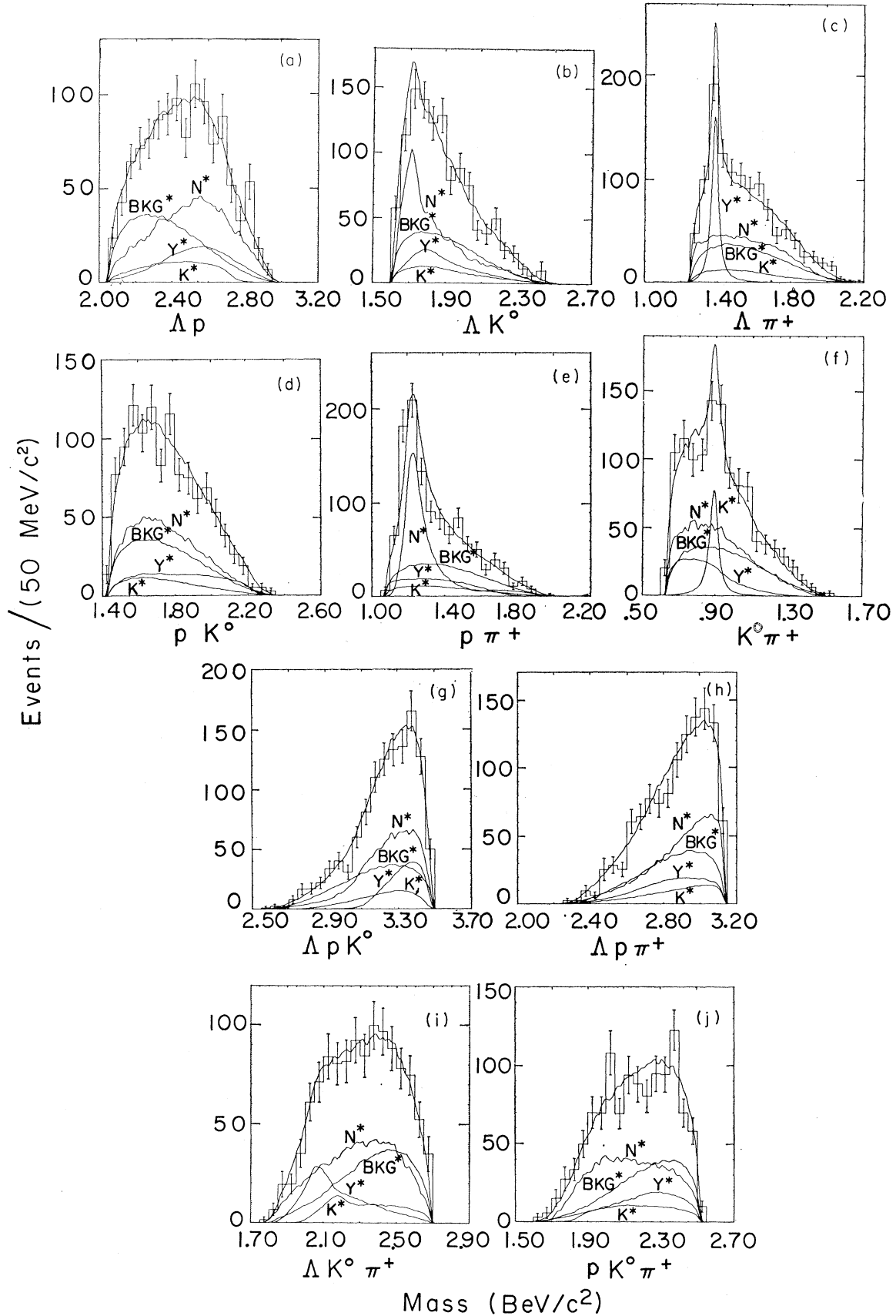


FIG. 12. Effective-mass distributions for all two-body and three-body combinations in the final state  $\Lambda p K^0 \pi^+$ . The curves superimposed on the experimental histograms are pion-exchange-model predictions, calculated with Monte Carlo methods.

We will discuss only the  $\Lambda p K^0 \pi^+$  final state since agreement with the model is somewhat better than for the other channels and the input data are of higher quality. This is the channel with the largest number of events and least contamination. As discussed above, the low- $K^0 \pi^+$ -effective-mass region is not fitted well by the model. The fit to the  $p \pi^+$  effective mass, shown in Fig. 12(e), has been shown to be improved by inclusion of off-mass-shell corrections, such as those of Dürr and Pilkuhn.<sup>16</sup> These tend to shift the resonance peak to a slightly lower value and result also in a somewhat narrower effective width for the resonance.

Further, more critical tests of the adequacy of the one-meson-exchange model were made by comparing angular distributions with predictions. This is a sensible procedure only if there exist reasonably accurate on-mass-shell pion reaction data. As discussed above, this is true only for the  $\Lambda p K^0 \pi^+$  state. In Figs. 13 and 14, we plot the angular distributions of the proton in the  $p \pi^+$  rest system and the  $\Lambda$  in the  $\Lambda K^0$  rest system. The reference direction in both cases is the momentum transfer to the two-body system. Satisfactory agreement is obtained. Thus the off-mass-shell scattering and produc-

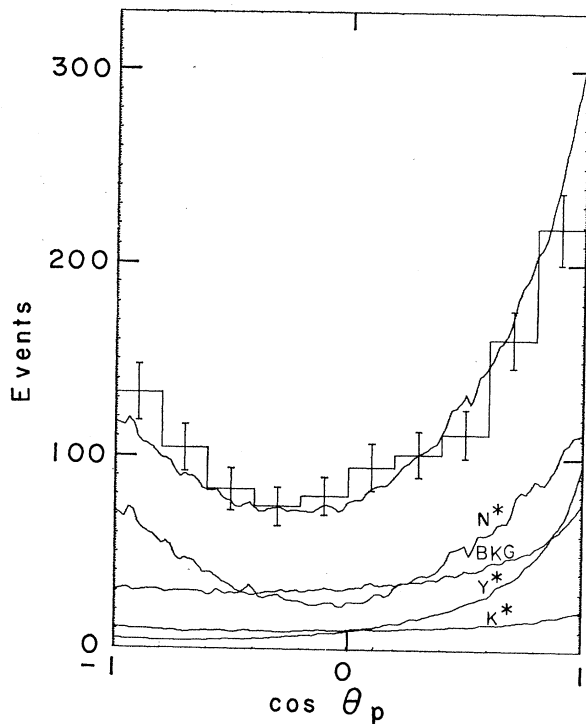


FIG. 13. Angular distribution of the proton in the  $p \pi^+$  rest system for the final state  $\Lambda p K^0 \pi^+$ . The angle  $\theta_p$  is between the proton direction and the momentum transfer to the  $p \pi^+$  system. The curves show pion-exchange predictions.

<sup>16</sup> H. P. Dürr and H. Pilkuhn, Nuovo Cimento 40, 899 (1965).

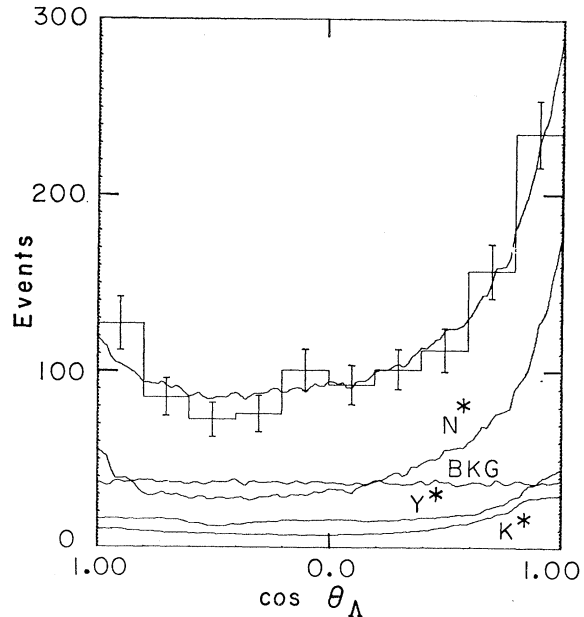


FIG. 14. Angular distribution of the  $\Lambda$  in the  $\Lambda K^0$  rest system for the final state  $\Lambda p K^0 \pi^+$ . The angle  $\theta_\Lambda$  is between the  $\Lambda$  direction and the momentum transfer to the  $\Lambda K^0$  system.

tion angular distributions are well represented by on-mass-shell experimental data.

Another test of the model is the Treiman-Yang angular distributions. We compute the angle between the

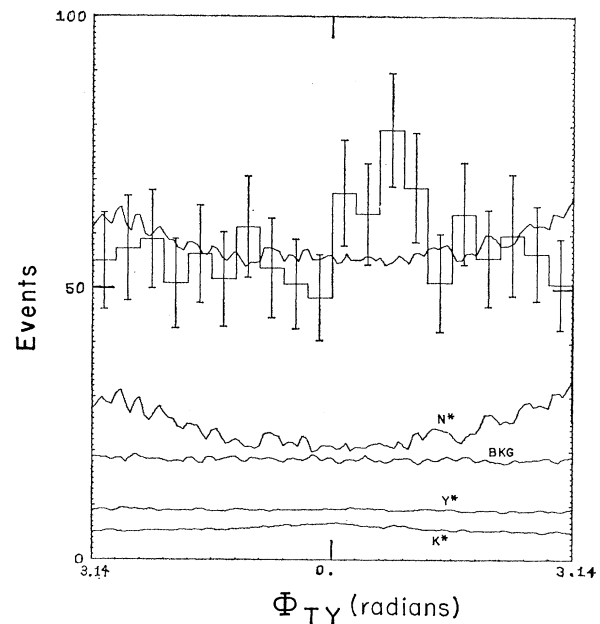


FIG. 15. Distribution of the Treiman-Yang angle for examples of the reaction  $pp \rightarrow \Lambda p K^0 \pi^+$ . The angle  $\Phi_{TY}$  is between the plane containing the incident and final protons and a plane containing the  $K$  momentum and the momentum transfer to the  $\Lambda K \pi$  system, calculated in the  $\Lambda K \pi$  rest system. The curves show the pion-exchange-model prediction.

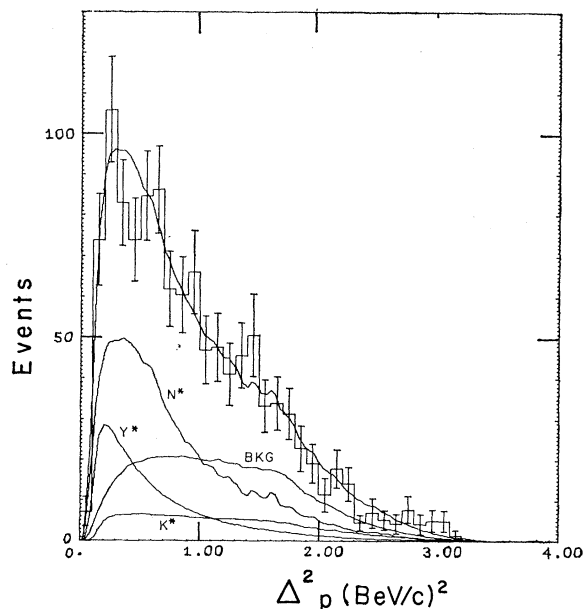


FIG. 16. Distribution of square of four-momentum transfer to the proton in the reaction  $p p \rightarrow \Lambda p K^0 \pi^+$ . The curves show the pion-exchange-model predictions.

normal to the plane containing the  $K$  momentum and momentum transfer in the  $\Lambda K \pi$  center-of-mass system and the normal to the plane of the incident and recoil

nucleons. This angle has the meaning of the usual Treiman-Yang angle for those events which are produced by the exchange diagram 7(b) and so has a simple distribution for those events not containing  $N^*$ . All events are included in the distributions shown in Fig. 15. The curves shown include the effects of diagram 7(a), i.e., they include the distribution in this angle for events containing  $N^*(1236)$  as well. Comparison with theory of the Treiman-Yang distribution for all events is therefore a test of the entire model. Again agreement with the model is quite good. Finally, in Fig. 16 we show the distribution in momentum transfer to the final-state proton for all events identified as  $\Lambda p K^0 \pi^+$ . The data are well fitted by the model over the complete range of momentum transfer. Similar results are observed in the other final states supporting the conclusion that the data are well represented by the one-pion-exchange model.

## VI. CONCLUSIONS

Resonance production via quasi-two-body and three-body channels contribute strongly to strange-particle production in four-body final states. A simple one-pion-exchange mechanism including empirical form factors gives predictions in good agreement with the data.